CHEMPHYSCHEM

DOI: 10.1002/cphc.200600308

Computationally-Assisted Approach to the Vibrational Spectra of Molecular Crystals: Study of Hydrogen-Bonding and Pseudo-Polymorphism**

Mariela M. Nolasco,[a] Ana M. Amado,[b] and Paulo J. A. Ribeiro-Claro*[a]

A new computationally-assisted methodology (PiMM), which accounts for the effects of intermolecular interactions in the crystal, is applied to the complete assignment of the Raman and infrared vibrational spectra of room temperature forms of crystalline caffeine, theobromine, and theophylline. The vibrational shifts due to crystal packing interactions are evaluated from ab initio calculations for a set of suitable molecular pairs, using the B3LYP/6-31G approach.The proposed methodology provides an answer to the current demand for a reliable assignment of the vibrational spectra of these methyl-xanthines, and clarifies several misleading assignments. The most relevant intermolecular interactions in each system and their effect on the vibrational spectra are considered and discussed. Based on these results, significant insights are obtained for the structure of caffeine in the anhydrous form (stable at room temperature), for which no X-ray structure has been reported. A possible structure based on $C_{(8)}$—H···$N_{(9)}$ and $C_{(1,3)}$—H···O intermolecular interactions is suggested.*

1. Introduction

Caffeine (1,3,7-trimethylpurine-2,6-dione; **CA**), theophylline (1,3-dimethylpurine-2,6-dione; **TP**), and theobromine (3,7-dimethylpurine-2,6-dione; **TB**) are three methylated xanthine derivatives (see Figure 1) widely found in the human diet that represent three different systems of important pharmaceutical interest. They naturally occur in food products such as tea, coffee, and cocoa beans (with TB and CA being the two most abundant xanthines in chocolate, for instance). On the other hand, these compounds are also used in a variety of medical applications, being routinely prescribed. For instance, CA is used as a central nervous system, cardiac and respiratory stimulant, while TP and TB are widely used as smooth muscle relaxants.

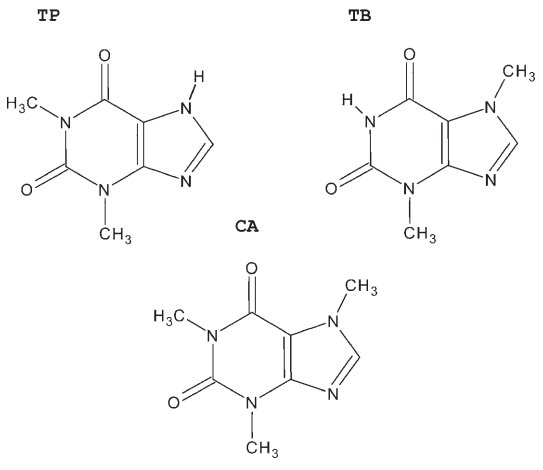

Figure 1. Schematic representation of the xanthine derivatives: theophylline (TP), theobromine (TB), and caffeine (CA).

TP is also used as a bronchodilator, for the treatment of bronchial asthma and neonatal apneia[1] and in the treatment of epilepsy.[2] All three compounds are also known to cause diuresis,[3] while CA administration seems to protect mice against a whole-body lethal dose of γ-irradiation.[4]

The polymorphic behavior of drugs is a major concern of the pharmaceutical industry since different packing arrangements of the same molecular species (polymorphism) can have markedly different biopharmaceutical properties.[5] It is well documented that CA and TP are sensitive to polymorphic and pseudo-polymorphic transformations that affect their dissolution profiles and, consequently, their bioavailability.[6–11] In fact, they crystallize into different states (hydrate and anhydrous)[12–15] and are good model compounds for the accurate characterization of both the polymorphic form and hydration states.

In this way, the knowledge of the structural characteristics of these compounds from a molecular point of view is of utmost relevance for a rational understanding of the structure-activity

[a] *Dr. M. M. Nolasco, Prof. P. J. A. Ribeiro-Claro*
CICECO, Departamento de Química
Universidade de Aveiro, 3810-193 Aveiro (Portugal)
Fax: (+351) 234 370 084
E-mail: pclaro@dq.ua.pt

[b] *Dr. A. M. Amado*
Química-Física Molecular, Departamento de Química
FCTUC, Universidade de Coimbra
3004-535 Coimbra (Portugal)
Fax: (+351) 239 826 541

[**] *in Theophylline, Theobromine, and Caffeine.*

relationship ruling their biochemical effects. In this context, the analysis of the vibrational spectra (Raman and FTIR), in particular of CA and TP, has aroused considerable interest.[6,16–22] However, to the best of our knowledge, no complete vibrational assignment has been attempted yet and the complete and reliable assignment of the vibrational spectra of these compounds is naturally justified. Very recently some works showed the vibrational spectra of CA, TP, and TB,[6,12,19–21,23] but, unfortunately, including incomplete, questionable and even misleading assignments, as reported previously by some of us.[22]

The complete assignment of the vibrational spectra of relatively complex molecules in the crystalline state is quite difficult, and the assignment of some experimentally observed bands to specific vibrations is usually uncertain. In order to assist this difficulty, theoretical calculations are used to support a reliable assignment by comparing the theoretically calculated spectra with the experimentally observed ones. The usefulness of theoretical calculations, particularly using density functional theory (DFT) methods, to assist vibrational spectroscopic studies has been recently highlighted.[24]

The present paper has been organized as follows. Firstly, the PiMM methodology (Pairs in Molecular Materials) is presented. Secondly, the results are discussed in two sections 1) the description of the crystal structures of xanthine derivatives based on ab initio calculations at the B3LYP/6-31G* level; 2) the complete assignment, based on the computationally-assisted methodology, of the FT-Raman and FTIR spectra of TB, TP, and CA and their pseudopolymorphs.

2. Results and Discussion

2.1. Methodology

The computationally-assisted methodology for vibrational spectra assignment used is based on the frequency and intensity calculations, for fully-optimized geometry structures, at the B3LYP/6-31G* level. This approach—vibrational spectra assignment by comparison with suitable simulated spectra—has been successfully applied for a couple of systems[25–28] and is generally recognized as a reliable approach.[24] On the other hand, the B3LYP/6-31G* level is known to provide a good "quality/computational cost ratio" for both geometry optimizations and vibrational spectra simulations in organic systems.

The major limitation of ab initio calculations in what concerns the prediction of the vibrational spectra arises from the complexity of the calculations involved, which imposes severe limitations on the size of the system. Despite the development of computers, it is still difficult to deal with systems of more than a few dozens of atoms. In this way, most of the frequency and intensity calculations refer to the single molecule situation. The calculated spectrum for the single molecule is expected to describe the gas phase spectra, and can be used with caution to simulate liquid phase and solution spectra, but fails to describe properly the solid-state spectra. The error is as large as the strong intermolecular interactions in the solid state.

A possible approach to overcome this limitation, proposed in this work, is to assume that the intermolecular interactions in the crystal perturb the wavenumbers of the isolated molecule. Within this approach, the wavenumber of the *i*th normal mode is given by its calculated wavenumber in the isolated molecule, corrected for the perturbations resulting from the contacts with neighbouring molecules in the crystal as represented in Equation (1):

$$\nu_i(\text{crystal}) = \nu_i(\text{isolated}) + \sum \Delta\nu_i^{(1)}(\text{direct}) + \sum \Delta\nu_i^{(1)}(\text{indirect}) + \sum \Delta\nu_i^{(2)}(\text{direct}) + \sum \Delta\nu_i^{(2)}(\text{indirect}) + \ldots \quad (1)$$

where the term "direct" refers to the effect of the intermolecular contacts on the oscillators involved in the contact (e.g. the effect of a O–H···O hydrogen bond on the O-H vibrational modes), while the term "indirect" refers to the effect of the same contact on the remaining modes (e.g. the effect of a O–H···O hydrogen bond on the modes involving oscillators in other parts of the molecule), and the summation applies to all possible contacts. The superscripts (1), (2) apply respectively to the first and second shell of neighbors.

Assuming that only the neighbors in the first shell significantly affect the calculated wavenumbers of the isolated molecule, Equation (1) simplifies to [Eq. (2)]

$$\nu_i(\text{crystal}) = \nu_i(\text{isolated}) + \sum \Delta\nu_i^{(1)}(\text{direct}) + \sum \Delta\nu_i^{(1)}(\text{indirect}) \quad (2)$$

and the corrections can be obtained by frequency calculations for all the molecular pairs required to describe the different intermolecular contacts present in the crystal (after full-geometry optimization).

The simplified version shown in Equation (2) neglects the effects of long-range interactions and the cooperativity of the various interactions. Although it is difficult to fully quantify the importance of these effects, it can be estimated by comparing the results for molecular pairs with those obtained for larger associations of molecules. From a set of calculations performed for associations of three and four molecules, these effects are estimated to affect the predicted shifts, on average, by less than $\approx 5\ cm^{-1}$. However, differences of $\approx 25–35\ cm^{-1}$ are observed in the most sensitive modes.

2.2. Selection of Relevant Molecular Pairs from the Crystal Structures

The crystal structures of the three methyl xanthines considered, present networks of hydrogen bonds which are expected to have a significant effect on the corresponding vibrational spectra.[13–15,29–33] The application of the previously described methodology requires ab initio calculations on molecular pairs that simulate the molecular associations found in the solid structures. In the case of TP and CA, the crystal structures of both hydrate forms (hereafter named TPh and CAh, respectively) and anhydrate forms (hereafter named TPa and CAa, respectively) must be considered, while for TB only the anhy-

drous form (hereafter named TBa) is known to exist. It is to be noted, however, that the crystal structure of anhydrous CA (known to exist as two different polymorphic forms, namely α- and β-forms[34]) has not been determined as only powders and disordered crystals are obtained.[35]

Figure 2 shows the most important intermolecular hydrogen bonds found in the crystal packing of the methyl-xanthine derivatives studied. Each interaction is described by one of the

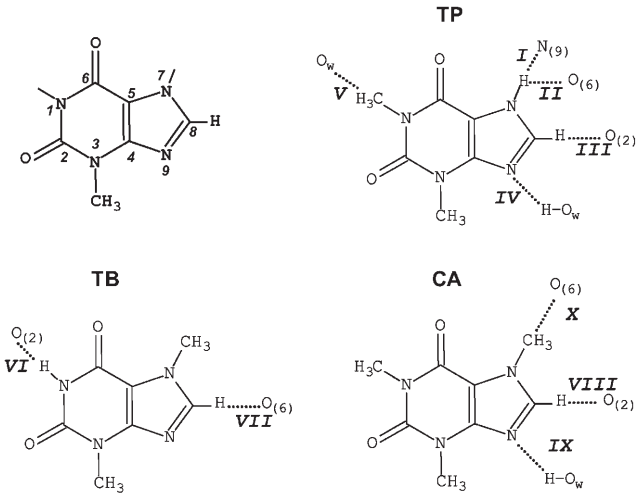

Figure 2. Atom numbering of xanthine derivatives and schematic representation of the molecular pairs with relevant intermolecular contacts observed in the crystal structures retrieved from the Cambridge Structural Database (ref. code indicated): pair I (theophylline anydrous, BAPLOT01 [14]), pairs II-V(theophylline hydrate, THEOPH/THEOPH01 [29]), pairs VI and VII (theobromine anydrous, SEDNAQ [13]), pairs VII-X (caffeine hydrate, CAFINE/CAFINE01 [30]). O_w represents the oxygen atom from the water molecule.

molecular pairs I–X indicated (for instance, molecular pair I is built from two TP molecules linked by a $N_{(7)}$–H···$N_{(9)}$ hydrogen bond). Among the methyl-xanthine derivatives considered, TP is the one for which the crystal structures of both forms (anhydrate and hydrate) are known. Thus, TP is the best model to demonstrate the application of the computationally-assisted methodology proposed. In this context, the packing analysis of the crystal structures of TPh and TPa forms, and the ab initio studies required to describe the intermolecular contacts present in each case, are discussed in more detail.

2.2.1. Theophylline

The crystal structures of both TPh and TPa forms show that all groups but one are involved in intermolecular hydrogen bonding, although there are significant differences in the donor/acceptor pairing between the two forms. The exception is the methyl group at position $N_{(3)}$, which does not participate in any hydrogen bond neither in the hydrate structure nor in the anhydrous structure. A characteristic feature of the monohydrated structure is the existence of heaped layers of dimeric structures of TP molecules, related by a centre of symmetry, which are held together by two types of TP···TP interactions, namely $N_{(7)}$–H···$O_{(6)}$ and $C_{(8)}$–H···$O_{(2)}$ (each TP molecule establishing two equivalent interactions of each type, thus acting both as a donor and as an acceptor). In addition, each TP molecule establishes two types of TP···H_2O interactions ($N_{(9)}$···H–O_w and $C_{(1)}$–H···O_w), forming water network channels that cross the different TP molecular layers. In turn, the crystal structure of the anhydrous form has no defined layers. In fact, the planar TP molecules are stacked in columns, where the interplanar angle between adjacent TP molecules of 43°. These columns are held together by $N_{(7)}$–H···$N_{(9)}$ hydrogen bonds.

Figure 2 presents the optimized structures of the different TP molecular pairs that simulate the different intermolecular interactions (TP···TP and TP···H_2O) present in the solid structures of either TPh or TPa forms. In all cases, the calculated intermolecular distance of the interaction is indicated. It should be mentioned that the TP molecule can occur in four tautomeric forms, namely TP($N_{(7)}$H), TP($N_{(9)}$H), TP($O_{(2)}$H), and TP($O_{(6)}$H). However, the X-ray results demonstrate that in the crystalline state, the TP($N_{(7)}$H) tautomer is prevalent.[14] Moreover, the ab initio calculations are in agreement with this observation, since the energy difference between the lowest-energy tautomeric form TP($N_{(7)}$H) and the second most stable form [TP($N_{(9)}$H)] is larger than 38 kJ mol^{-1}. In this way, all the molecular pairs in Figure 3 were built up from the TP($N_{(7)}$H) tautomeric form.

Molecular pair I represents the intermolecular contacts characteristic of the TPa form (TP dimer structures held by $N_{(7)}$–H···$N_{(9)}$ interactions), while molecular pairs II, III, IV, and V represent the four distinct molecular associations that are evident in the TPh crystal structure (molecular associations held through $N_{(7)}$–H···$O_{(6)}$ and $C_{(8)}$–H···$O_{(2)}$, $N_{(9)}$···H–O_w and $C_{(1)}$–H···O_w interactions). Molecular pair II, which presents two strong $N_{(7)}$-H···$O_{(6)}$ interactions, corresponds to the lowest energy minimum found. The predicted N–H···O distance is 177 ppm, which is in good agreement with the reported X-ray value, 190 ppm,[29] taking into account the distinct nature of the two methods. Molecular pair III, which is built by a weaker intermolecular interaction ($C_{(8)}$–H···$O_{(2)}$), corresponds to the less stable TP···TP dimer. Despite their weakness, C–H···O hydrogen bonds are known to play a significant role in crystal packing and have major effects on the vibrational spectra of molecular systems.[25,27,28]

Table 1 presents the predicted ab initio wavenumbers for the TP monomer and the wavenumber shifts promoted by considering the different molecular pairs of Figure 3 (only the modes that are significantly affected by the intermolecular contacts are shown).

2.2.2. Theobromine and Caffeine

Figures 4 and 5 show the molecular pairs which characterize the crystal structures of TBa and CAh, respectively. Starting with the TBa, a characteristic feature of its crystal structure is the association of TB molecules resulting in pseudo-centrosymmetric structures linked by two intermolecular $N_{(1)}$–H···$O_{(2)}$ hydrogen bonds (molecular pair VI of Figure 4).[13] These molecular pairs are held together through weaker $C_{(8)}$–H···$O_{(6)}$ hydrogen bonds between adjacent molecules (molecular pair VII in Figure 4), forming a two-dimensional layered structure.

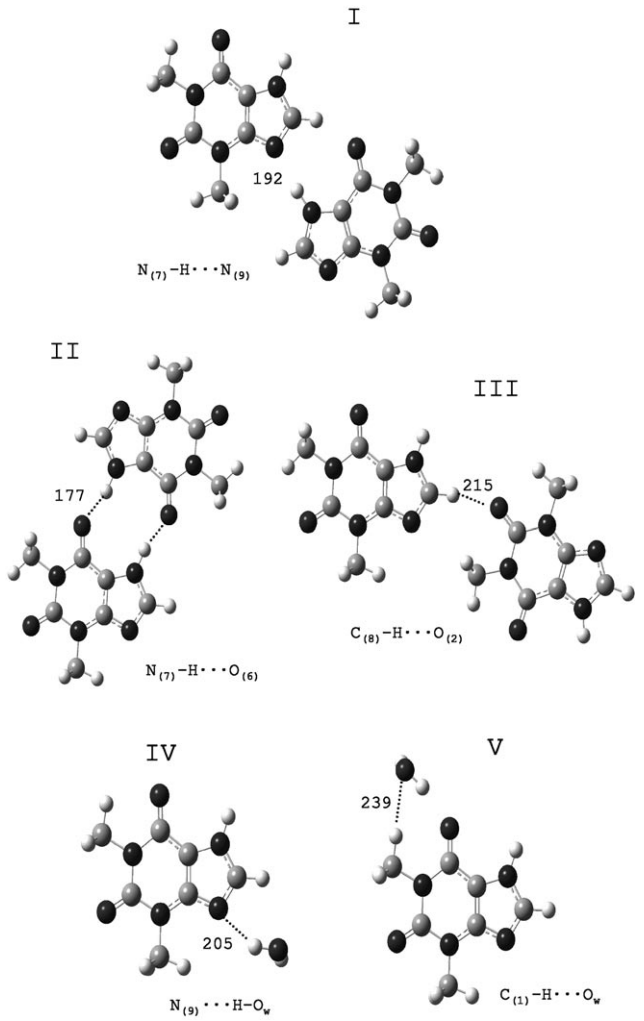

Figure 3. Optimized structures of the molecular pairs selected to describe the intermolecular contacts in the crystal structure of theophylline anhydrous (TPa, pair I) and theophylline monohydrate (TPh, pairs II-V), showing the calculated H···N and H···O distances in pm.

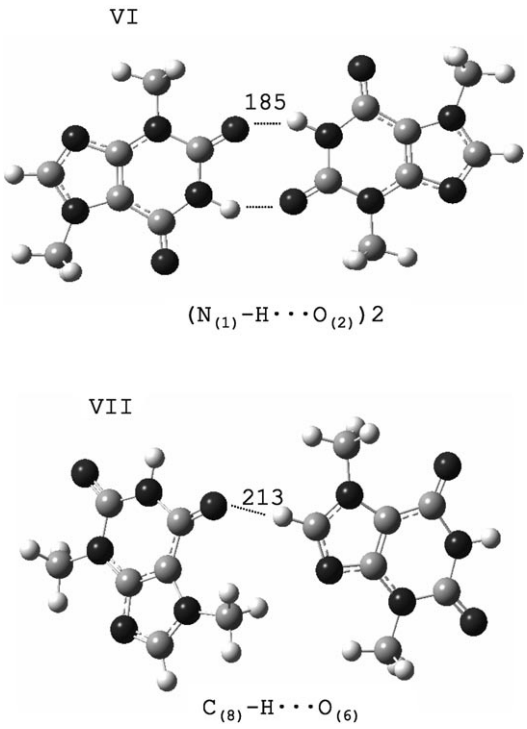

Figure 4. Optimized structures of the molecular pairs selected to describe the intermolecular contacts in the crystal structure of anhydrous theobromine (TBa). Calculated H···O distances in pm.

The crystal structure of the CAh was determined in 1958 by Sutor[30] and confirmed in 1997 by Edwards and co-workers.[12] In this structure, the imidazole nitrogen atom of the CA molecule establishes a hydrogen bond with a water molecule of crystallization, $N_{(9)}$···H–O_w (molecular pair IX of Figure 5). The water molecules are disordered and the distance between water oxygen atoms in the channel is only 2.5 Å.[35]

The strong $N_{(9)}$···H-O_w hydrogen bond results in the activation of the neighboring $C_{(8)}$–H as hydrogen bond donor.[14] In the crystal structure of CAh, the $C_{(8)}$···$O_{(2)}$ intermolecular distance is 3.1 Å (and consequently, H···$O_{(2)}$ distance ≈2.1 Å).[10,12] This evidences the existence of molecular pairs kept by $C_{(8)}$–H···$O_{(2)}$ hydrogen bonds (molecular pair VIII of Figure 5). Additionally, there is also proof of molecular pairing through $C_{(7)}$–H···$O_{(6)}$ (represented by the molecular pair X of Figure 5). The calculated stabilizing effect of these molecular associations follows the order IX > VIII > X, in agreement with the results of Carlucci and Gavezzoti, using a higher level of calculations.[35] It also follows the expected pat-

Table 1. Ab initio calculated wavenumbers for theophylline monomer and the different molecular associates based on the X-ray structure of theophylline anhydrous (TPa) and hydrate (TPh). Only shifts > 10 cm^{-1} are shown.

Monomer	Predicted wavenumber shifts/cm^{-1}						Approximate description[a]
	TPa	TPh					
	I	II	III	IV	V	Sum (II-V)	
363	10	17	10			27	βC=O
446		14				14	α pyr ring
501	324	319		22		341	$\gamma N_{(7)}$–H
538		16				16	pyr ring breath
800	87	43	76	42		161	$\gamma C_{(8)}$–H
1092	66	58	−10	−19	−20	9	νCC + νCN
1217	180	25	165			190	$\beta C_{(8)}$–H
1381	−154	−148				−148	$\beta N_{(7)}$–H
1538	11	13				13	νCC + νCN
1585		−15				−15	$\nu C_{(4)}$=$C_{(5)}$
1694		−33	−14		−13	−60	νC=O
3153	−27		−14			−14	$\nu C_{(8)}$–H
3509	−384	−336				−336	$\nu N_{(7)}$–H

[a] ν = stretching; β = in-plane deformation; γ = out-of-plane deformation; α = in-plane ring deformation; pyr = pyrimidine.

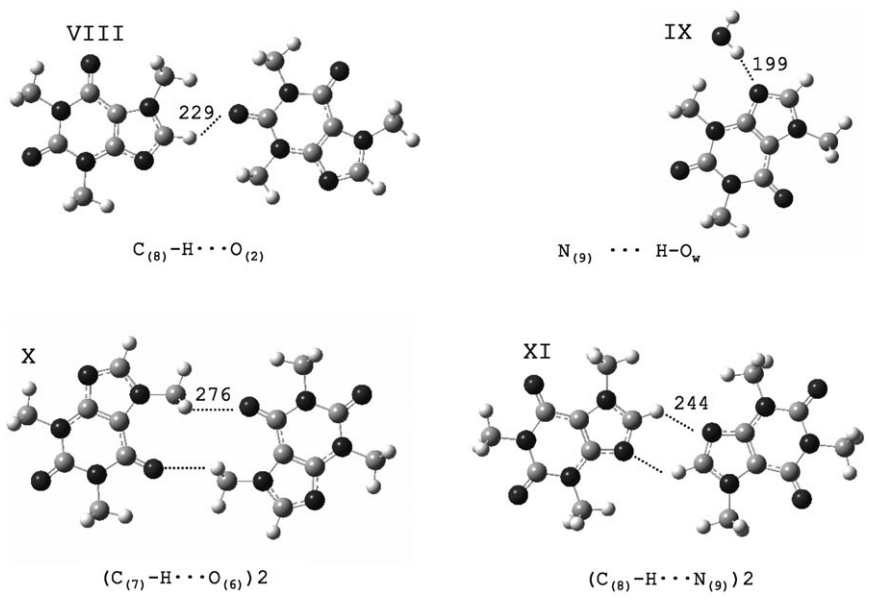

Figure 5. Optimized structures of the molecular pairs selected to describe the intermolecular contacts in the crystal structure of caffeine monohydrate (CAh, pairs VIII-X). Also included is the molecular pair XI describing a possible intermolecular contact in the anhydrous caffeine form (CAa). Calculated H···N and H···O distances in pm.

tern of the intermolecular interaction strength, $N_{(9)}$···H–O_w > $C_{(8)}$–H···$O_{(2)}$ > $C_{(7)}$–H···$O_{(6)}$.

In the CAa form, the $N_{(9)}$-atom is no longer blocked by the water molecule and can be used by another H-bond donor group. In order to assess new insights into the possible structure of CAa crystal, several other molecular associations, presenting the $N_{(9)}$-atom as the H-bond acceptor, are tested. A relevant one is the association of two CA molecules by weak $C_{(8)}$–H···$N_{(9)}$ hydrogen bonds (molecular pair XI of Figure 5), due to its stabilization energy. This molecular pair has already been considered among the most probable in crystalline CAa by Carlucci and Gavezzoti, although these authors do not assign any structure-driving importance to weak C–H···O/N bonds.[35]

Tables 2 and 3 present the predicted ab initio wavenumbers for the monomer and the wavenumber shifts promoted by considering the different molecular pairs for TB and CA forms, respectively (only the modes that are significantly affected by the intermolecular contacts are shown).

2.3. Vibrational Assignments Using the Computationally Assisted Methodology

In this section, the complete assignment of the FT-Raman and FTIR spectra of the three methyl-xanthine derivatives is presented in the light of the above discussed structural features, namely, the effect of the intermolecular interactions present in each system through Equation (2). It should be mentioned that due to the strong coupling of oscillators in some normal modes, the approximate description of the modes presented below is based on the highest contribution for each vibrational mode. In a few cases, the unavoidable hybrid nature of the vibrational mode is indicated in the approximate description with a plus sign (e.g. νCC + νCN modes).

2.3.1. Theophylline

The application of Equation (2) to TP is straightforward for the modes listed in Table 1, as the predicted wavenumbers for each normal mode are obtained by simply adding the predicted shifts to the calculated value for the monomer. For instance, considering the βC=O mode—first line of Table 1—its predicted wavenumbers are 363 + 10 = 373 cm^{-1} for TPa and 363 + 27 = 390 cm^{-1} for TPh. Thus, this mode is assigned to the observed bands at 377 and 388 cm^{-1} in the Raman spectra of TPa and TPh, respectively. The same procedure is applied to the modes presenting smaller shifts and not shown in Table 1.

Figure 6 compares the experimental and calculated (for the isolated TP molecule and for the different molecular pairs considered) FT-Raman spectra of TPa and TPh in the 1000-1800 cm^{-1} region (the complete IR and Raman spectra of both TP forms are published elsewhere[22]). The application of the computationally-assisted methodology in the assignment of the vibrational spectra is also illustrated, since the 1000–1800 cm^{-1} wavenumber region is particularly sensitive to the structural differences between TPa and TPh. As can be seen from Figure 6, there are a number of spectral changes on going from the predicted

Table 2. Ab initio calculated wavenumbers for theobromine monomer (TBa) and the two molecular associates based on the X-ray structure of theobromine anhydrous (TBa). Only shifts > 10 cm^{-1} are shown.

Monomer	Predicted wavenumber shifts/cm^{-1} TBa			Approximate description[a]
	VI	VII	Sum(VI+VII)	
151	10		10	butterfly
213		12	12	βN(7)–C(H_3)
229		10	10	δ pyr ring
400	15		15	βC=O
685	−18		−18	γC=O
624	251		251	γN(1)H
802		76	76	γC(8)H
1214		13	13	βC(8)H
1305	15		15	νCC + νCN
1356	71		71	βN(1)H
1475	10	13	23	δ_{as}C(3)H_3
1486	−11	−10	−21	δ_{as}C(7)H_3
1725	−33	−24	−57	νC=O
1738	−10	−11	−21	νC=O
3468	−284		−284	νN(1)H

[a] ν = stretching; β = in-plane deformation; γ = out-of-plane deformation; α = in-plane ring deformation; pyr = pyrimidine.

Table 3. Ab initio calculated wavenumbers for caffeine monomer and the different molecular associates based on the X-ray structure of caffeine anhydrous (CAa) and hydrated (CAh). Only shifts > 10 cm^{-1} are shown.

Monomer	Predicted wavenumber shifts/cm^{-1}					Approximate description[a]
	CAh				CAa	
	VIII	IX	X	Sum(VIII-X)	XI	
297		14		14		βN(3)–C(H_3)
801	58		10	68	58	γC(8)H
1055		11		11		ρC(7)H3 + νN(1)C(H_3)
1221					12	βC(8)H
1687	−15		−10	−25		νC=O
3143					−19	νC(8)H

[a] ν = stretching; β = in-plane deformation; γ = out-of-plane deformation; ρ = CH_3 rocking.

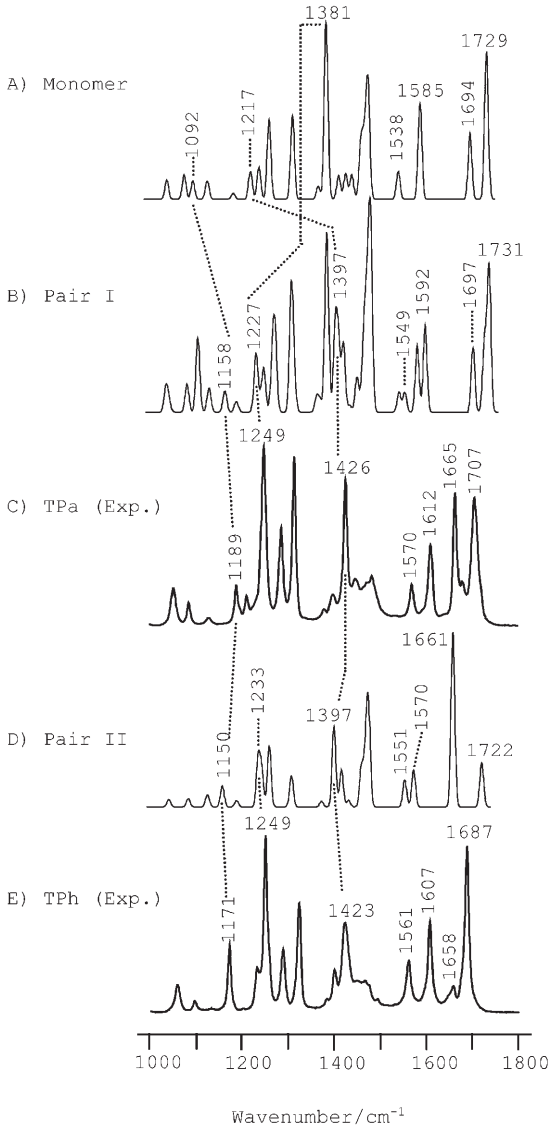

Figure 6. Example of methodology with theophylline anhydrous (TPa) and theophylline monohydrate (TPh). Calculated and experimental Raman spectra in the 1000-1800 cm^{-1} region of theophylline monomer (A), molecular pair I (B), TPa (C), molecular pair II (D), and TPh (E).

single molecule (frame A) to molecular pairs I and II (frame B and D, respectively). Considering the information presented in Table 1, the most sensitive modes present in the 1000–1800 cm^{-1} spectral region are the νC=O, $\nu C_{(4)}=C_{(5)}$, νCC + νCN, $\beta C_{(8)}H$, and $\beta N_{(7)}H$ vibrational modes. The carbonyl stretching bands (νC=O) predicted for the monomer (1694 and 1729 cm^{-1}) are not significantly affected in molecular pair I (frame B) but are clearly shifted downwards (to 1661 and 1722 cm^{-1}) in molecular pair II (frame D). This shift of the carbonyl stretching modes towards lower frequencies in molecular pair II is explained by the presence of a strong $N_{(7)}$-H···$O_{(6)}$ hydrogen bond engaging the $C_{(6)}$=O group. Molecular pair III (not included in Figure 6) also exhibits carbonyl stretching modes shifted to lower frequencies (1680 and 1726 cm^{-1}) due to the presence of weak $C_{(8)}H$···$O_{(2)}$ hydrogen bonding. Based on this data, the two carbonyl modes of TPh can be related to the pair of bands at 1658-1687 cm^{-1} (frame E). The corresponding modes for TPa are ascribed to the 1665-1707 cm^{-1} pair (frame C), somewhat far from the monomer values. This is one of the rare cases in which the limitations of the method become more evident: the νC=O modes in TPa seem to be affected by long-range interactions not included in Equation (2).

The in-plane bending modes of the $N_{(7)}H$ and $C_{(8)}H$ groups ($\beta N_{(7)}H$ and $\beta C_{(8)}H$, respectively) are predicted to occur in the monomer (frame A) at 1381 and 1217 cm^{-1}, respectively. However, the formation of the intermolecular interactions $N_{(7)}H$···$N_{(9)}$ (molecular pair I) and $N_{(7)}H$···$O_{(6)}$ (molecular pair II) shifts the $\beta N_{(7)}H$ and $\beta C_{(8)}H$ to lower and higher frequencies, respectively. The $\beta N_{(7)}H$ is downward shifted as a direct consequence of the formation of the $N_{(7)}H$···$N_{(9)}$ or $N_{(7)}H$···$O_{(6)}$ interactions, while the upward shift predicted for the $\beta C_{(8)}H$ is an indirect consequence of those interactions [an example of the indirect effect of intermolecular interactions, as described in Equation (2)]. Additionally, in the molecular pair III, the $\beta C_{(8)}H$ mode is also shifted to higher frequency, almost to the same extent, due to the formation of weaker $C_{(8)}H$···$O_{(2)}$ hydrogen bonding. Based on these results, the experimentally observed band at 1249 cm^{-1} in the Raman spectra of both TPa and TPh (frame C and E, respectively) can be assigned to the $\beta N_{(7)}H$ mode. On the other hand, the $\beta C_{(8)}H$ mode appears at 1426 cm^{-1} for the TPa form (frame C), being shifted to 1423 cm^{-1} on hydrate formation (frame E).

A comparison of the experimental Raman spectra of both forms (frames C and E) shows that the bands at 1612 ($\nu C_{(4)}=C_{(5)}$) and 1570 cm^{-1} (νCC + νCN) are shifted to 1607 and 1561 cm^{-1}, respectively, upon hydrate formation. Another important criterion for the assignments herein proposed is the isotopic vibrational shifts upon N-H deuteration. Ab initio calculations show that besides the three N-H modes (νNH, βNH,

γNH) other modes include the motion of the H atom at $N_{(7)}$ and thus are significantly affected by the H/D exchange.

The FT-IR spectra of TPa, TPh, and TPh_{-d} (hydrated deuterated TP) in the 500-1000 and 2000-3600 cm^{-1} regions are shown in Figure 7. A comparison of the FT-IR spectra in Figure 7 shows the presence of a broad band at 846 cm^{-1} (TPa, frame A) that is shifted to 818 cm^{-1} upon hydration (TPh, frame B) and disappears upon crystallization in D_2O, being shifted to 593 cm^{-1} (TPh_{-d}, frame C). These bands are clearly ascribed to the out-of-plane bending mode of $N_{(7)}$–H ($\gamma N_{(7)}$–H). The observed wavenumber shift from TPa to TPh suggests that the the $N_{(7)}H\cdots N$ hydrogen bond in the TPa is stronger than the $N_{(7)}H\cdots O(6)$ hydrogen bond in TPh.

The analysis of the infrared spectrum in the 2000-3600 cm^{-1} region is somewhat restricted by the strong broad bands due to the H_2O and D_2O stretching modes and the Fermi resonance effects. The FT-IR of TPh evidences a well-defined band at 3139 cm^{-1}, which is absent in the spectrum of TPh_{-d}. The spectrum of TPh_{-d}, on the other hand, shows a new band at 2495 cm^{-1}, within the range of the predicted isotopic shift. Consequently, it is reasonable to assign these two bands to the $N_{(7)}$–H and $N_{(7)}$–D stretching vibrations, respectively. This vibrational mode ($\nu N_{(7)}$–H) appears at 3061 cm^{-1} in the FTIR spectrum of TPa.

Figure 7 also illustrates the effects of the intermolecular interactions in the modes directly engaged in intermolecular contacts. This is particularly evident for those related to the $C_{(8)}$–H group, which is engaged in C–H···O hydrogen bonding in TPh. According to the vibrational frequency calculations, it is reasonable to ascribe the $C_{(8)}$–H stretching mode ($\nu C_{(8)}$–H) to the bands observed at 3106 and 3122 cm^{-1} in the spectra of TPh and TPa, respectively. This indicates a red-shift upon hydrogen bonding, characteristic of strong C–H donors.[36]

From the vibrational modes analysis (see Table 1) it is predicted that the $C_{(8)}$–H out-of-plane bending mode ($\gamma C_{(8)}$–H) in TPh crystal should appear at $\approx$160 cm^{-1} above the 800 cm^{-1} predicted for the monomer. The strong band observed at 980 cm^{-1} in the FT-IR spectrum of TPh, in a region where all the remaining bands can be reasonably assigned to other vibrational modes, is thus designated to the $\gamma C_{(8)}$–H mode. In TPa, the same vibrational mode is predicted to occur at somewhat lower frequency (ca. $800+87$ cm^{-1}, Table 1), but is found at nearly the same frequency as for TPh. This can be viewed as the error limit of the method, although there is a qualitative agreement in the sense that the $\gamma C_{(8)}$–H mode is significantly upward shifted from the monomer values in both TPa and TPh forms.

The complete assignment of the Raman and FT-IR spectra of TPa and TPh—resulting from all the data gathered and the considerations above—is presented in Table 4. Apart from the expected fundamental modes, small contaminations with the metastable polymorph of TP (TP_m) can be found in the vibrational spectra.[11]

2.3.2. Theobromine and Caffeine

The experimental wavenumbers and proposed assignments of TBa and of CAa and CAh are summarized in Tables 5 and 6, respectively.

As stated above (and shown in Table 2), in the case of TBa the main intermolecular interactions are of the type $N_{(1)}H\cdots O_{(2)}$ and $C_{(8)}H\cdots O_{(6)}$. Therefore, it is expected that the most affected vibrational modes are the ones related to the $C_{(2)}$=O and $C_{(6)}$=O carbonyl groups, and to the $N_{(1)}H$ and $C_{(8)}H$ groups. In fact, according to ab initio calculations the νC=O modes are shifted to lower frequencies upon formation of those intermolecular interactions, the effect being naturally larger in the case of the stronger $N_{(1)}H\cdots O_{(2)}$ interaction ($\Delta\nu = 33$ cm^{-1} and $\Delta\nu = 24$ cm^{-1} on passing from monomer to molecular pair VI and to molecular pair VII, respectively). On the other hand, the out-of-plane C=O (γC=O) mode is predicted to shift from 685 cm^{-1} for the monomer to 667 cm^{-1} for molecular pair VI and to 688 cm^{-1} for molecular pair VII.

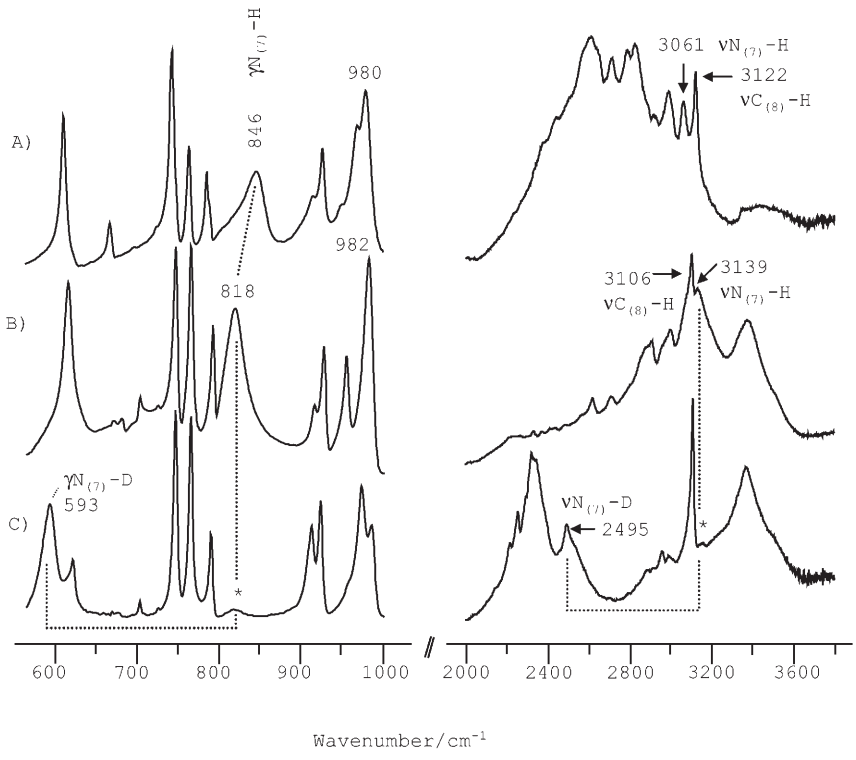

Figure 7. Infrared spectra of TPa (A), TPh (B), and TPh_{-d} (C) in the 500-1000 and 2000-3600 cm^{-1} regions, with the assignments based on the isotopic shift. The weak features marked with (*) in spectrum C are due to the residual presence of non-deuterated TPh.

Table 4. Complete computationally-assisted assignments of the FT-Raman and FT-IR spectra of theophylline anhydrous (TPa) and hydrate (TPh).

TPa Calc[b]	Raman	FTIR	TPh Calc[b]	Raman	FTIR	Approximate description[a]
112	117	–	*173*	–	–	$\tau C_{(1)}H_3$
129	132	–	*116*	–	–	$\gamma N_{(1)}$–CH_3
150	164	–	*167*	179	–	Butterfly motion
193	211	–	*191*	192	–	ζ pyr
293	305	–	*293*	294	–	ζ pyr + $\beta N_{(3)}$–CH_3
319	326	–	*350*	328	–	$\beta N_{(1)}$–CH_3
346	363	363	*368*	369	369	ζ pyr
373	377	377	*390*	388	390	βC=O
419	–	420	*437*	–	420	βC=O
446	447	445	*460*	453	455	α pyr
501	504	503	*503*	502	499	α pyr
538	555	–	*554*	572	–	Pyr breathing
–	578	–	–	–	–	TP_m
591	612	611	*605*	614	615	ζ imid
656	668	668	*674*	673	675	α pyr
–	676	–	–	–	–	TP_m
672	698	697	*674*	702	702	γC=O
709	743	742	*709*	747	746	ζ imid
717	765	763	*711*	765	765	γC=O
773	786	785	*772*	790	792	νCC + νCN
–	789	789	–	–	–	TP_m
825	850	846	*842*	–	818	$\gamma N_{(7)}$–H
–	915	–	–	–	–	TP_m
908	928	–	*908*	918	–	α imid
944	950	950	*946*	–	955	α imid
971	970	970	*975*	962	–	$\rho C_{(1)}H_3$(ip)
887	982	980	*961*	986	982	$\gamma C_{(8)}$–H
1036	1052	1049	*1039*	1058	1056	$\nu N_{(3)}$–CH_3
1076	1085	1085	*1143*	1096	1092	$\nu N_{(1)}$–CH_3
–	1094	1095	–	–	–	TP_m
1126	1130	1126	*1126*	1133	1130	$\rho C_{(3,1)}H_3$(oop)
–	1170	–	–	–	–	TP_m
1158	1189	1188	*1101*	1171	1165	νCC + νNC
1185	–	1195	*1187*	–	1199	$\rho C_{(3)}H_3$(ip)
1236	1212	–	*1247*	1231	–	νCC + νNC
–	1225	–	–	–	–	TP_m
1227	1249	1242	*1233*	1249	1245	$\beta N_{(7)}$–H
–	–	1249	–	–	–	TP_m
1260	1287	1284	*1258*	1288	1287	νCC + νNC
1309	1315	1314	*1309*	1322	1321	νCC + νNC
–	–	1319	–	–	–	TP_m
1364	1399	1397	*1377*	1399	1397	imid breathing
1397	1426	1425	*1407*	1423	1420	$\beta C_{(8)}$–H
1445	1448	1446	*1460*	1448	1445	νCC + νCN
1457	1464	1468	*1464*	1465	1461	$\delta_{as} C_{(3,1)}H_3$
1477	1484	1484	*1470*	1494	1492	$\delta_{as} C_{(3)}H_3$
1549	1570	1565	*1560*	1561	1556	νCC + νCN
1585	1612	1608	*1571*	1607	1606	$\nu C_{(4)}$=$C_{(5)}$
1697	1665	1665	*1634*	1658	1665	νC=O
–	1681	1678	–	–	–	TP_m
1728	1707	1713	*1718*	1687	1692	νC=O
2964	2968	–	*2966*	2962	2967	$\nu_{as} C_{(1,3)}H_3$
3074	3032	–	*3074*	3010	3003	$\nu_{as} C_{(1,3)}H_3$
3126	3123	3122	*3139*	3109	3106	$\nu C_{(8)}$–H
3125	–	3061	*3173*	–	3139	$\nu N_{(7)}$–H
–	–	–	–	3377	3379	ν_{as}OH (H_2O)

[a] ν = stretching; β = in-plane deformation; γ = out-of-plane deformation; α = in-plane ring deformation; ζ = out-of-plane ring deformation; δ = CH_3 deformation; ρ = CH_3 rocking; τ = CH_3 torsion. TP_m = small contamination with metastable TP form; pyr = pyrimidine, imid = imidazole; [b] Calculated values using Equation (2) (monomer + predicted shifts).

Figure 8 shows the calculated infrared spectra (in the 550-950 cm^{-1} region) of TB monomer (frame A), molecular pair VI (frame B), and molecular pair VII (frame C). The $\gamma N_{(1)}H$ and $\gamma C_{(8)}H$ vibrational modes are expected to occur in this spectral region. The $\gamma N_{(1)}H$ mode is predicted at 624 cm^{-1} for the monomer, being significantly shifted upwards (to 875 cm^{-1}) upon establishment of the $N_{(1)}H\cdots O_{(2)}$ hydrogen bond (molecular pair VI). On the other hand, the $\gamma C_{(8)}H$ mode is predicted to shift upwards by $\approx$79 cm^{-1} when the weaker $C_{(8)}H\cdots O_{(6)}$ interaction is considered (molecular pair VII). As both types of interactions are present in the crystal structure of TBa, it is expected that both the $\gamma N_{(1)}$–H and $\gamma C_{(8)}$–H modes are observed in the 800-900 cm^{-1} region.

The stretching vibrations of $C_{(8)}$–H and $N_{(1)}$–H ($\nu C_{(8)}$–H and $\nu N_{(1)}$–H, respectively) are also affected by the presence of the $N_{(1)}$–$H\cdots O_{(2)}$ and $C_{(8)}$–$H\cdots O_{(6)}$ hydrogen bondings. According to the calculations both modes are shifted to lower frequencies on passing from the monomer to one of the two molecular pairs (VI or VII). Based on this information and on the deuteration studies, the $\nu N_{(1)}$–H mode was ascribed to a broad band at 3156 cm^{-1} in the FT-IR spectrum, while a band centered at 3116 cm^{-1} in the Raman spectrum was assigned to the $\nu C_{(8)}$–H mode.

As for TP, deuteration studies are used to confirm the assignment of the bands due to the N–H modes in TBa. Figure 9 compares part of the FT-Raman and FT-IR spectra of TBa and TBa_{-d} (partially deuterated TBa). As can be seen, there is a clear intensity decrease of the broad band observed at 862 cm^{-1} in the FT-IR spectrum upon partial deuteration. Thus, it is reasonable to ascribe this band to the

Table 5. Complete computationally-assisted assignment of the FT-Raman and FT-IR spectra of theobromine anhydrous.

Calc[a]	Raman	FTIR	Approximate description[b]
123	117	–	$\gamma N_{(7)}$–CH_3
161	169	–	Butterfly motion
209	188	–	ζ pyr
225	225	–	$\beta N_{(7)}$–CH_3
239	256	–	ζ pyr
313	321	–	$\beta N_{(3)}$–CH_3
370	375	373	ζ pyr + βC=O
415	415	420	βC=O
460	460	456	α pyr
496	509	507	α pyr
591	621	615	pyr breathing + ζ imid
665	675	680	α pyr
667	696	691	γC=O
705	734	732	νCC + νCN
713	751	751	γC=O
723	766	763	ζ imid
764	778	783	α imid
876	–	862	$\gamma N_{(1)}$–H
876	888	888	$\gamma C_{(8)}$–H
926	946	940	α imid
1025	1040	1040	$\nu N_{(3)}$–CH_3
1056	1072	1071	$\rho C_{(7)}H_3$(ip)
1122	1138	1140	νCC + νCN + $\rho C_{(7,3)}H_3$(oop)
1160	1177	1172	νCC + νCN
1200	1208	1204	$\rho C_{(3)}H_3$(ip)
1227	1226	1225	$\beta C_{(8)}$–H
1275	1298	1294	νCC + νCN
1320	1334	1334	νCC + νCN
1346	1363	1365	$\nu N_{(7)}$–CH_3
1379	1394	1392	Imid breathing
1426	1411	1410	$\beta N_{(1)}$–H
1422	1426	1424	$\delta_{as} C_{(7,3)}H_3$
1450	1455	1455	$\delta_{as} C_{(7)}H_3$ + νCC + νCN + $\delta_{as} C_{(3)}H_3$
1498	1480	1480	$\delta_{as} C_{(3)}H_3$
1465	1489	1486	$\delta_{as} C_{(7)}H_3$
1534	1552	1548	νCC + νCN
1572	1594	1592	$\nu C_{(4)}$=$C_{(5)}$
1668	1685	1690	νC=O
1717	1708	1710	νC=O
2966	2956	2951	$\nu_{as} C_{(7,3)}H_3$
3023	3002	3001	$\nu_{as} C_{(3)}H_3$
3040	3025	3025	$\nu_{as} C_{(7)}H_3$
3073	3037	3040	$\nu_{as} C_{(3)}H_3$
3144	3116	3117	$\nu C_{(8)}$–H
3184	3157	3156	$\nu N_{(1)}$–H

[a] Calculated values using Equation (2) (monomer + predicted shifts) [b] ν = stretching; β = in-plane deformation; γ = out-of-plane deformation; α = in-plane ring deformation; ζ = out-of-plane ring deformation; $\delta = CH_3$ deformation; $\rho = CH_3$ rocking; $\tau = CH_3$ torsion; pyr = pyrimidine, imid = imidazole.

Table 6. Complete computationally-assisted assignment of the FT-Raman and FT-IR spectra of caffeine anhydrous (CAa) and hydrate (CAh).

CAa			CAh			Approximate description[a]
Calc[b]	Raman	FTIR	Calc[b]	Raman	FTIR	
124	106	–	*120*	109	–	$\gamma N_{(7)}$–CH_3
128	143	–	*130*	128	–	$\gamma N_{(1)}$–CH_3
164	164	–	*174*	168	–	Butterfly motion
212	227	–	*222*	217	–	$\beta N_{(7)}$–CH_3
219	235	–	*227*	238	–	ζ_p pyr
277	282	–	*281*	292	–	ζ pyr
297	315	–	*311*	319	–	$\beta N_{(3)}$–CH_3
359	373	371	*359*	375	373	$\beta N_{(1)}$–CH_3 + ζ pyr
398	391	390	*398*	389	388	βC=O
413	425	425	*409*	–	425	βC=O
446	445	444	*453*	447	444	α pyr
487	484	481	*491*	487	481	α pyr
536	556	–	*538*	556	–	pyr breathing
602	610	609	*604*	612	612	ζ imid
625	644	644	*630*	647	647	α pyr
672	698	700	*671*	699	700	γC=O
718	742	745	*718*	744	745	ζ imid + γC=O
729	–	759	*728*	762	762	νCC + νCN
785	802	800	*785*	805	803	νCC + νCN
859	863	860	*869*	888	888	γC(8)–H
912	929	927	*915*	929	926	α imid
961	976	974	*959*	978	975	α imid
1009	1023	1026	*1010*	1027	1026	$\rho C_{(1)}H_3$(ip)
1055	1072	1070	*1066*	1076	1075	$\rho C_{(7)}H_3$(ip) + $\nu N_{(1)}$-CH_3
1114	1134	1130	*1109*	1130	1130	$\rho C_{(7,1,3)}H_3$(oop)
1181	1190	1187	*1170*	1192	1192	$\rho C_{(3)}H_3$(ip)
1202	1212	1212	*1198*	1214	1212	$\nu N_{(3)}$–CH_3
1233	1241	1239	*1221*	1242	1239	$\beta C_{(8)}$–H
1238	1251	–	*1236*	1256	1257	νCC + νCN
1265	1285	1286	*1260*	1290	1289	νCC + νCN
1316	1329	1326	*1320*	1333	1329	νCC + νCN
1341	1361	1358	*1353*	1361	1359	$\nu N_{(7)}$–CH_3
1375	1390	1390	*1373*	1392	1391	imid breathing
1405	1404	1401	*1405*	1410	1412	$\delta_{as} C_{(1,7)}H_3$
1425	1431	1430	*1432*	1435	1432	$\delta_{as} C_{(3)}H_3$
1456	1458	1456	*1456*	1456	1455	$\delta_{as} C_{(7,3,1)}H_3$ + νCC + νCN
1472	1469	–	*1472*	1475	1471	$\delta_{as} C_{(1,3)}H_3$
1488	1491	1485	*1490*	–	1489	$\delta_{as} C_{(7)}H_3$
1532	1554	1549	*1534*	1553	1550	νCC + νCN
1578	1600	1599	*1570*	1606	1602	$\nu C_{(4)}$=$C_{(5)}$
1687	1656	1658	*1662*	1655	1658	νC=O
1722	1698	1701	*1715*	1698	1704	νC=O
2963	2959	2955	*2963*	2959	2955	$\nu_{as} C_{(1)}H_3$ + $\nu_{as} C_{(7)}H_3$ + $\nu_{as} C_{(3)}H_3$
3026	3017	–	*3028*	3011	3007	$\nu_{as} C_{(1)}H_3$
3029	3035	–	*3031*	3027	–	$\nu_{as} C_{(3)}H_3$
3124	3114	3111	*3143*	3122	3122	$\nu C_{(8)}$–H
–	–	–	–	–	3375	ν_{as}OH (H_2O)
–	–	–	–	3392	–	ν_{as}OH (H_2O)

[a] ν = stretching; β = in-plane deformation; γ = out-of-plane deformation; α = in-plane ring deformation; ζ = out-of-plane ring deformation; $\delta = CH_3$ deformation; $\rho = CH_3$ rocking; $\tau = CH_3$ torsion; pyr = pyrimidine, imid = imidazole. [b] Calculated values using Equation (2) (monomer + predicted shifts).

$\gamma N_{(1)}$–H. In addition, based on the ab initio results, the close-lying band at 888 cm^{-1} is assigned to the $\gamma C_{(8)}$–H mode.

It should be mentioned that there is an excellent agreement between the predicted shifts in Table 2 and those actually observed in the vibrational spectra of TBa (see Table 5). The only exception is the γC=O mode, whose predicted wavenumber is 685 ± 18 cm^{-1} and is observed at 691 cm^{-1}.

Caffeine (CA) presents a particular vibrational problem. In contrast to what is observed for TP and TB, the vibrational spectra of the anhydrous and monohydrated forms (CAa and CAh) are very similar, showing only slight intensity changes and/or frequency shifts for a few spectral features. The non-sensibility of the vibrational spectra to the crystal packing is also predicted by the ab initio calculations; as shown in Table 3, only a small number of modes are found to be affected by the intermolecular interactions considered.

Figure 10 illustrates this similarity, by comparing the FT-IR spectra of CAa (frame A) and CAh (frame B). As it can be seen,

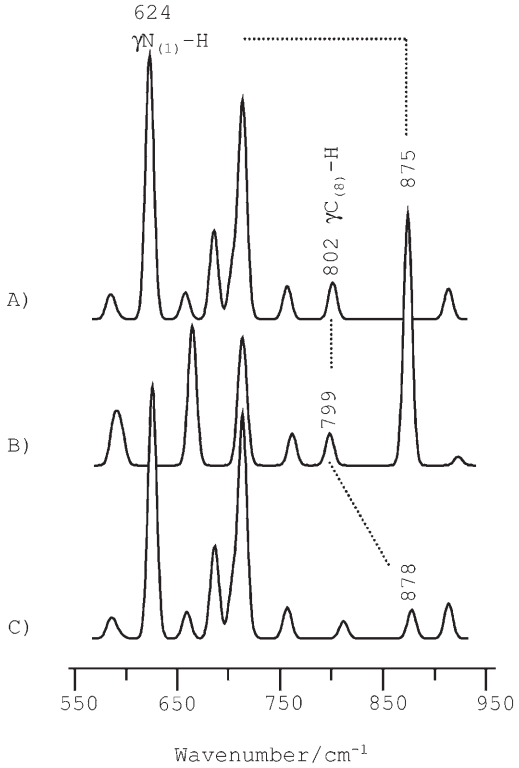

Figure 8. Calculated infrared spectra of TB in the 550-950 cm^{-1} region: monomer (A), molecular pair VI (B), and molecular pair VII (C)

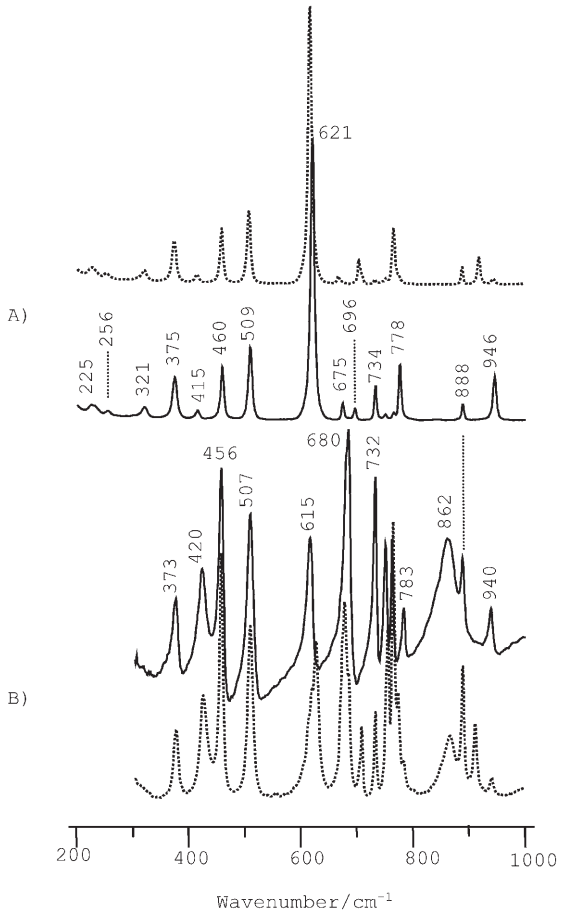

Figure 9. Raman (A) and FT-IR (B) spectra of TBa in the 200-1000 cm^{-1} region: normal TBa (——), deuterated TBa (-----).

the νC=O region remains nearly unchanged on passing from CAh to CAa, apart from the intensity increase of the higher wavenumber band. This observation suggests that the intermolecular interactions involving the carbonyl groups are not significantly different for the CAh and CAa forms.

A somewhat controversial spectral change occurs for the CAh band centred at 888 cm^{-1}. On passing from CAh (frame B) to CAa (frame A), this band disappears, giving rise to a broad spectral feature with maximum intensity at 860 cm^{-1}. The 888 cm^{-1} band has been ascribed to the H_2O libration mode by Edwards et al.[12] However, this assignment is not supported by our deuteration studies, as the band remains unchanged in the spectrum of CAh_{-d} (hydrated deuterated CA, spectrum not shown) when only D_2O molecules are present in the crystal. Based on the predicted shifts of Table 3, this band can be assigned to the $\gamma C_{(8)}$–H mode.

Another significant spectral change on passing from CAh to CAa is observed in the region of the $\nu C_{(8)}$–H mode. The band assigned to the $\nu C_{(8)}$–H mode is shifted downwards from ≈3122 cm^{-1} in CAh to ≈3114 cm^{-1} in CAa. This band shifting is followed by a significant intensity increase. These spectral changes upon dehydration are similar to

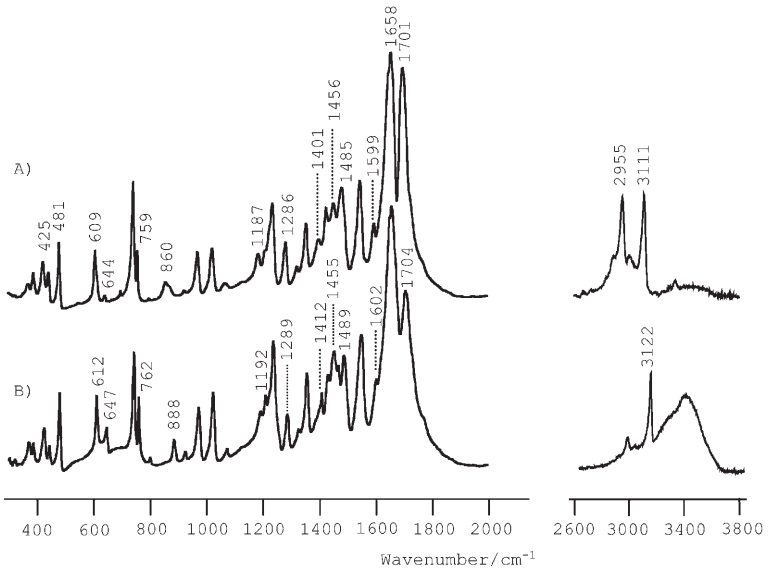

Figure 10. FT-IR spectra of CAa (A) and CAh (B) in the 350-2000 and 2600-3800 cm^{-1} regions.

those observed upon hydration in TP (downwards shifting from 3122 to 3106 cm^{-1} and considerable intensity increase). This comparison yields some clues concerning the intermolecular interaction patterns in the two forms (anhydrous and hydrate) of these systems.

On the whole, the spectral similarities between CAh and CAa seem to indicate that the intermolecular interaction patterns of the two forms are either similar in the donor/acceptor grouping or in the interaction strength. As no strong H-bond donor is available in CAa, the strongest hydrogen bond possible is of the type $C_{(8)}$-H···X, with X being either an O or an N atom, with the vibrational modes ascribed to the $C_{(8)}$–H group being sensitive to the interactions established by the close-lying $N_{(9)}$-group. Based on the ab initio calculations performed, there seems to be a higher stability upon formation of a $C_{(8)}$–H···$N_{(9)}$ interaction over a $C_{(8)}$–H···$O_{(2)}$ interaction. Thus, it is reasonable to assume that in the case of CAa the main intermolecular interaction is the van der Waals interaction, but with a contribution from a specific $C_{(8)}$–H···$N_{(9)}$ contact.

Attaining to the fact that the νC=O region remains almost unaffected on passing from CAh to CAa, it is also reasonable to consider the presence of weak $C_{(1)}$–H···$O_{(6)}$/$C_{(1)}$–H···$O_{(2)}$ or $C_{(3)}$–H···$O_{(6)}$/$C_{(3)}$–H···$O_{(2)}$ interactions in the CAa structure. The presence of these interactions explain to some extent the similarity observed in the carbonyl stretching bands of CAa and CAh and also the blue shifting of the carbon-hydrogen stretching mode involving the N-methyl group, namely the $\nu_{as}C(1)H_3$ and $\nu_{as}C(3)H_3$, on passing from CAh to CAa.

3. Conclusions

This study presents a new methodology (PiMM—Pairs in Molecular Materials) for the assignment of the vibrational spectra of molecular crystals, based on the ab initio evaluation of wavenumber shifts resulting from the intermolecular contacts.

The approach was tested on pharmacologically active methyl-xanthine derivatives, which are known to present pseudo-polymorphism and strong intermolecular interactions. It was found that the proposed methodology is simple, not computationally demanding, and yields reliable results. This methodology can be particularly useful in the detection and in the structural characterization of the solid-solid transformations which significantly affect the activity of a particular pharmaceutical drug.

The main errors of this methodology arise from 1) the neglecting of weak/long-range interactions and cooperativity effects, and 2) from the differences between the optimized geometry of the pairs and their arrangement in the crystal. These errors are clearly larger than those resulting from the limitations of the standard double-zeta basis set used. However, the number of inconsistencies or erroneous predictions (discussed through the text and shown in Tables 4–6) is quite low, considering the simplicity of the approach and the complexity of the systems.

A systematic investigation of both the pseudo-polymorphic transformations and intermolecular interactions occurring in theophylline, theobromine, and caffeine, as well as a complete and consistent assignment of their vibrational spectra was performed. Apart from solving some misleading assignments of the literature, this study clearly shows the relevance of vibrational spectroscopy coupled to ab initio calculations, for the study of pharmaceutical relevant drugs. As the vibrational motion is potentially different depending on the packing and conformational arrangement, the presence of different hydrogen bonds in theophylline, theobromine, and caffeine and their pseudo-polymorphs affect differently the vibrational wavenumbers, intensities, and shapes of some characteristic bands. It has been shown, as expected, that the most pseudo-polymorph-sensitive modes are related to the donor and acceptor groups involved in each intermolecular hydrogen bond. In fact, considering the overall results, the vibrational modes related with the C=O, N–H, and C–H groups, namely the νC=O, νN–H, νC–H, βC–H, βN–H, γN–H, and γC–H modes are strongly affected by intermolecular hydrogen bond formation. The study of the wavenumber shifts promoted by each contact also provides new insight into the crystal structure of caffeine anhydrous. We suggest that the presence of $C_{(8)}$–H···$N_{(9)}$ and $C_{(1,3)}$–H···O intermolecular interactions explain the differences between the vibrational spectra of hydrated and dehydrated forms of caffeine.

Experimental Section and Computational Methods

Sample Preparation: Anhydrous CA, TP. and TB were obtained commercially (Aldrich) and used without further purification. TPh was prepared by dissolving anhydrous TP in distilled water at 60 °C until a supersaturated solution was reached. The crystals obtained were filtered from the mother liquid, allowed to dry at room temperature and relative humidity conditions, and then gently milled to powder. Crystals of CAh were prepared by a similar process, but using a water-bath at 80 °C and stored in a sealed vessel at 92% relative humidity in the presence of potassium nitrate saturated solution at room temperature. The N-deuterated isotopomers were prepared by a similar process.

Vibrational Spectroscopy: The FT-Raman spectra in the 70–5000 cm^{-1} region were recorded on a RFS-100 Bruker FT-spectrometer, using a Nd:YAG laser with excitation wavelength of 1064 nm, with laser power set to 300 mW. Each spectrum is the averaging of two repeated measurements of 100 scans each and 2 cm^{-1} resolution.

Room-temperature FTIR spectra in the 300–4000 cm^{-1} region were recorded with a Mattson 7000 FTIR spectrometer, using a globar source, a deuterated triglycine sulphate (DTGS) detector, and potassium bromide cells. All spectra are the average of two counts, with 64 scans each, at 2 cm^{-1} resolution.

It was apparent that in some experiments the sample temperature rose significantly due to laser exposure, leading either to polymorphic transformations or loss of solvent molecules.[37,38] In order to evaluate this effect, a sample of TPh was exposed continuously to 300 mW laser power for 2 h, and 24 records of 5 min each were collected. The comparison of the spectra shows that the first spectral change, assignable to sample heating (denoting some loss of water molecules), although still extremely subtle, became only observable after 35 min of exposure to the laser. All the FT-Raman

spectra reported on this work (using the conditions described above) have been collected in 25 min or less.

Ab initio calculations: Density functional theory (DFT) calculations were performed using the Gaussian 03W program package (G03W).[39] The functional used throughout the calculations consist of a mixture of HF (Hartree–Fock) and DFT exchange functionals and the gradient-corrected functional of Lee, Yang, and Parr,[40] as proposed and parameterized by Becke (standard B3LYP option of G03W).[41]

All molecular structures were fully optimized using the standard all-electron 6-31G* basis set, using the gradient method.[42] Harmonic vibrational wavenumbers were calculated, using analytical second derivatives, for all optimized geometries in order to confirm the convergence to a minimum at the potential energy surface and to evaluate the zero-point vibrational energy corrections (ZPVE). The wavenumbers above 500 cm^{-1} were scaled by a factor of 0.9614.[43]

In order to simulate and estimate the effects of the intermolecular interactions observed in the crystal structure of both anhydrous and monohydrated forms of the three methyl-xanthine derivatives, the calculations were extended to different molecular pairs. Different molecular associates, built on the basis of the crystal structures xanthine···xanthine and xanthine···H_2O intermolecular interactions, were considered and submitted to full optimization in all cases. The vibrational assignments were based on the visualization of the atomic displacements. A possible crystal structure for the room-temperature phase of anhydrous caffeine can be found at Acta Cryst. 2002, A48 (Supl.), C265. However, contact with the authors (F. Stowasser and C. W. Lehmann) revealed that the description of intermolecular contacts in the crystal is not yet possible.

Acknowledgments

The authors acknowledge financial support from the Portuguese Foundation for Science and Technology (FCT)—Unidade de Química-Física Molecular and Laboratório Associado CICECO. MN also acknowledges FCT for a doctoral fellowship - SFRH/BD/18854/2004.

Keywords: ab initio calculations · crystals · IR spectroscopy · noncovalent interactions · polymorphism · Raman spectroscopy

[1] C. E. Johnson, S. VanDeKoppel, E. Myers, *Am. J. Health-Syst. Pharm.* **2005**, *62*, 2518–2520.
[2] N. Ates, D. Sahin, G. Ilbay, *Epilpsy Behav.* **2004**, *5*, 645–648.
[3] J. B. Thomas, J. H. Yen, M. M. Schantz, B. J. Porter, K. E. Sharpless, *J. Agric. Food Chem.* **2004**, *52*, 3259–3263.
[4] K. C. George, S. A. Hebbar, S. P. Kale, P. C. Kesavan, *J. Radiol. Prot.* **1999**, *19*, 171–176.
[5] G. Fini, *J. Raman Spectrosc.* **2004**, *35*, 335–337.
[6] A. Jørgensen, J. Rantanen, M. Karjalainen, L. Khriachtchev, E. Räsänen, J. Yliruusi, *Pharm. Res.* **2002**, *19*, 1285–1291.
[7] S. Airaksinen, M. Karjalainen, E. Räsänen, J. Rantanen, J. Yliruusi, *Int. J. Pharm.* **2004**, *276*, 129–141.
[8] C. M. Adeyeye, J. Rowley, D. Madu, M. Javadi, S. S. Sabnis, *Int. J. Pharm.* **1995**, *116*, 65–75.
[9] N. V. Phadnis, R. Suryanarayanan, *J. Pharm. Sci.* **1997**, *86(11)*, 1256–1263.
[10] E. Suihko, V. P. Lehto, J. Ketolainen, E. Laine, P. Paronen, *Int. J. Pharm.* **2001**, *217*, 225–236.
[11] A. M. Amado, M. M. Nolasco, P. J. A. Ribeiro-Claro, unpublished results.
[12] H. G. M. Edwards, E. Lawson, M. de Matas, L. Shields, P. York, *J. Chem. Soc., Perkin Trans. 2* **1997**, 1985–1990.
[13] K. A. Ford, Y. Ebisuzaki, P. D. Boyle, *Acta Crystallogr. Sect. C* **1998**, *54*, 1980–1983.
[14] Y. Ebisuzaki, P. D. Boyle, J. A. Smith, *Acta Crystallogr. Sect. C* **1997**, *53*, 777–779.
[15] C. Sun, D. Zhou, D. J. W. Grant, V. G. Young Jr, *Acta Crystallogr. Sect. E* **2002**, *58*, 368–370.
[16] J. de Taeye, Th. Zeegers-Huyskens, *Spectrosc. Lett.* **1986**, *19(4)*, 299–310.
[17] S. Tarulli, E. J. Baran, *J. Raman Spectrosc.* **1993**, *24*, 139–141.
[18] R. A. Nyquist, S. L. Fiedler, *Vib. Spectrosc.* **1995**, *8*, 365–386.
[19] I. Pavel, A. Szeghalmi, D. Moigno, S. Cîntă, W. Kiefer, *Biopolymers* **2003**, *72*, 25–37.
[20] S. Gunasekaran, G. Sankari, S. Ponnusamy, *Spectrochim. Acta A* **2005**, *61*, 117–127.
[21] H. G. M. Edwards, T. Munshi, M. Anstis, *Spectrochim. Acta A* **2005**, *61*, 1453–1459.
[22] P. J. A. Ribeiro-Claro, A. M. Amado, *Spectrochim. Acta A* **2005**, *61*, 2796–2797.
[23] M. de Matas, H. G. M. Edwards, E. E. Lawson, L. Shields, P. York, *J. Mol. Struct.* **1998**, *440*, 97–104.
[24] M. Schmitt, J. Popp, *J. Raman Spectrosc.* **2006**, *37*, 20–28.
[25] M. M. Nolasco, P. J. A. Ribeiro-Claro, *ChemPhysChem* **2005**, *6*, 496–502.
[26] P. D. Vaz, P. J. A. Ribeiro-Claro, *Eur. J. Inorg. Chem.* **2005**, 1836–1840.
[27] H. I. S. Nogueira, S. M. J. Cruz, P. C. R. Soares-Santos, P. J. A. Ribeiro-Claro, T. Trindade, *J. Raman Spectrosc.* **2003**, *34*, 350–356.
[28] A. M. Amado, M. P. M. Marques, P. J. A. Ribeiro-Claro, *ChemPhysChem* **2002**, *3*, 599–606.
[29] D. J. Sutor, *Acta Crystallogr.* **1958**, *11*, 83–87.
[30] D. J. Sutor, *Acta Crystallogr.* **1958**, *11*, 453–458.
[31] E. Suihko, J. Ketolainen, A. Poso, M. Ahlgren, J. Gynther, P. Paronen, *Int. J. Pharm.* **1997**, *158*, 47–55.
[32] A. A Naqvi, G. C. Bhattacharyya, *J. Appl.Crystallogr.* **1981**, *14*, 464–464.
[33] E. D. L. Smith, R. B. Hammond, M. J. Jones, K. J. Roberts, J. B. O. Mitchell, S. L. Price, R. K. Harris, D. C. Apperley, J. C. Cherryman, R. Docherty, *J. Phys. Chem. B* **2001**, *105*, 5818–5826.
[34] H. Bothe, H. K. Cammenga, *Thermochim. Acta* **1980**, *40*, 29–39.
[35] L. Carlucci, A. Gavezzotti, *Chem. Eur. J.* **2005**, *11*, 271–279.
[36] P. J. A. Ribeiro-Claro, P. D. Vaz, *Chem. Phys. Lett.* **2004**, *390*, 358–361.
[37] J. Johansson, S. Pettersson, L. S. Taylor, *J. Pharm. Biomed. Anal.* **2002**, *30*, 1223–1231.
[38] N. A. Marigheto, E. K. Kemsley, J. Potter, P. S. Belton, R. H. Wilson, *Spectrochim. Acta A* **1996**, *52*, 1571–1579.
[39] Gaussian 03, Revision B.04, M. J. Frisch, G. W. Trucks, H. B. Schlegel, G. E. Scuseria, M. A. Robb, J. R. Cheeseman, J. A. Montgomery Jr, T. Vreven, K. N. Kudin, J. C. Burant, J. M. Millam, S. S. Iyengar, J. Tomasi, V. Barone, B. Mennucci, M. Cossi, G. Scalmani, N. Rega, G. A. Petersson, H. Nakatsuji, M. Hada, M. Ehara, K. Toyota, R. Fukuda, J. Hasegawa, M. Ishida, T. Nakajima, Y. Honda, O. Kitao, H. Nakai, M. Klene, X. Li, J. E. Knox, H. P. Hratchian, J. B. Cross, C. Adamo, J. Jaramillo, R. Gomperts, R. E. Stratmann, O. Yazyev, A. J. Austin, R. Cammi, C. Pomelli, J. W. Ochterski, P. Y. Ayala, K. Morokuma, G. A. Voth, P. Salvador, J. J. Dannenberg, V. G. Zakrzewski, S. Dapprich, A. D. Daniels, M. C. Strain, O. Farkas, D. K. Malick, A. D. Rabuck, K. Raghavachari, J. B. Foresman, J. V. Ortiz, Q. Cui, A. G. Baboul, S. Clifford, J. Cioslowski, B. B. Stefanov, G. Liu, A. Liashenko, P. Piskorz, I. Komaromi, R. L. Martin, D. J. Fox, T. Keith, M. A. Al-Laham, C. Y. Peng, A. Nanayakkara, M. Challacombe, P. M. W. Gill, B. Johnson, W. Chen, M. W. Wong, C. Gonzalez, J. A. Pople, Gaussian, Inc., Pittsburgh PA, **2003**.
[40] C. Lee, W. Yang, R. G. Parr, *Phys. Rev. B* **1988**, *37*, 785–789.
[41] A. Becke, *J. Chem. Phys.* **1993**, *98*, 5648–5652.
[42] P. C. Hariharan, J. A. Pople, *Theor. Chim. Acta* **1973**, *28*, 213–222.
[43] A. P. Scott, L. Radom, *J. Phys. Chem.* **1996**, *100*, 16502–16513.

Received: May 19, 2006
Revised: June 19, 2006
Published online on September 19, 2006

